Estimation of local failure in large tensegrity structures via substructuring using Interacting Particle-Ensemble Kalman Filter

Neha Aswal, Subhamoy Sen, Laurent Mevel

Estimation of local failure in large tensegrity structures via substructuring using Interacting Particle-Ensemble Kalman Filter

Neha Aswal[1 [0000−0003−3923−3592]], Subhamoy Sen[1 [0000−0001−8021−6693]], and Laurent Mevel[2 [0000−0001−8913−7393]]

[1] Indian Institute of Technology Mandi, Himachal Pradesh, India
[2] Univ. Gustave Eiffel, Inria, Cosys-SII, I4S, Campus de Beaulieu, France
nehaaswal96@gmail.com, subhamoy@iitmandi.ac.in, laurent.mevel@inria.fr

Abstract. Tensegrity is a network of bars and cables that maintains its structural integrity with tension present in its cables. Other than typical structural failure mechanisms, tensegrity may fail due to slacking of cables or buckling of bars. Real-life tensegrities are an assemblage of component modules. Large tensegrities require excessive computation for model-based structural health monitoring (SHM), which may sometimes make the problem ill-posed. Instead of the entire domain, only a sub-structure can be investigated explicitly. Substructures decouple the structure into independent components that can be monitored individually, provided the sub-domain interface is measured. Yet the integration of substructures within predictor-corrector model-based SHM algorithms needs special investigation from consistency, stability, and accuracy perspectives. To consider system uncertainties Bayesian filtering-based SHM approaches have been employed in this study. The need for interface measurement has been circumvented through an output injection approach. To increase computational efficiency, the domain decomposition approach is coupled with an interacting filtering-based approach that employs Ensemble Kalman filter (for state estimation) within an envelope of Particle filter (for health parameter estimation). This facilitates simultaneous estimation of state and parameters while enabling full parallelization capability.

The proposed approach is tested on a six-stage tensegrity tower made of component simplex modules.

Keywords: Tensegrity · Substructuring · Structural Health Monitoring · Interacting Particle Ensemble Kalman Filter · Damage Detection.

1 Introduction

Tensegrity structures/mechanisms are an assembly of compression elements (struts/ bars) afloat in a network of tension elements (cables). Tensegrities are characterized

by the presence of at least one infinitesimal mechanism stabilized by the prestress present in the cables, and the existence of multiple stable configurations. To accommodate external load, a tensegrity may change its configuration from one stable state to another leading to a change in its global stiffness. Evidently, tensegrity can have different stiffness for the same undamaged configuration due to difference in the prestress levels [1]. This is not common with regular structures where alteration in stiffness is considered a clear sign of damage, rendering structural health monitoring (SHM) for tensegrities a complicated problem. Besides, uncertainties due to unknown input force, model, measurement, etc. affect tensegrity SHM to the same extent as they affect the regular SHM problems. A probabilistic SHM approach can therefore be a practical solution in this regard.

Bayesian filtering approaches have been established as a good alternative for similar objectives in several researches. Bayesian filters, such as Kalman filter (KF), define system dynamics in state-space form with two probabilistic models, i.e., process and measurement. A set of unobserved system state defines the system dynamics by evolving in time through Chapman-Kolmogorov belief propagation strategy. The updated states are then observed through a measurement model mapping states to measurable responses. The predicted measurement when compared to the actual measurement gives the error/innovation which updates/corrects the propagated state estimate through Bayes' inferencing. By augmenting the health parameters/indices (**HI**s) along side the regular state, damage in the structure can be estimated simultaneously. However, **HI**s inducted additionally into the state vector eventually need a nonlinear mapping (measurement model) to be observed, making the SHM problem nonlinear.

Nonlinear filter variants, such as, Extended (EKF), Unscented (UKF), Ensemble (EnKF) Kalman filters and Particle filter (PF) have been successfully employed in the literature for state and damage estimation. However augmentation of the health indices increases the dimensionality of the state, thereby increasing the computation cost. Interacting filtering strategies, like interacting particle Kalman filter (IPKF), have been a breakthrough in this endeavor in which PF estimates the parameters while KF, nestled inside the PF, estimates the state variables [2,3]. However, since both the process and measurement models for tensegrity are nonlinear, KF needs to be replaced by EnKF [4] for SHM of tensegrity.

Real-life tensegrities are complex and large compared to the simpler tensegrity modules (simplex, octahedron, etc.). With model based approach in which a recursive simulation call is mandatory, involvement of a high dimensional model may render the approach computationally uneconomical. Moreover extracting measurement data (acceleration, strain, etc.) from all the element members is tedious and impractical. Substructure identification techniques significantly reduce the resources required for SHM by analysing the structure in parts; first part being the elements critical to the overall health of the structure.

Initially employed for system identification via model reduction approach [5], substructuring is also effective for the SHM of large complex structures [6]. Similar to structural dynamics, substructuring can be described in physical (mass, stiffness, etc.), frequency (fourier transform) or modal (eigen value decomposition) domain. The substructures are predominantly defined in modal domain [6] with a few exceptions [7]. Typically with these approaches, the interfaces need to be measured extensively which is not always possible due to accessibility constraints. Further, in real-life problems, the input is hardly known/measured either explicitly or statistically, and therefore mostly estimated as additional states [8,9], which however makes the estimable state dimension larger.

The current study focuses on local SHM of tensegrity (requires nonlinear modelling) with the help of substructuring in physical/time domain wherein interface/ boundary forces are rejected by employing output injection technique [2,3], which substantially reduces the sensor, equipment, etc. requirement and computational cost.

2 System Model

Tensegrity members undergo large deformation under external loading, which can be modelled by introducing geometric nonlinearity to the finite element modeling (FEM). In this article an explicit representation of the strain-displacement relationship is adopted following [4], which gives the locally linearized tangent stiffness matrix, $\mathbf{K}^m(t)$ as follows,

$$\mathbf{K}^m(t) = \frac{A^m l^m}{2} \int_{-1}^{1} \frac{\partial(\mathbf{B}^{m\,T} \sigma^m(r,t))}{\partial \mathbf{q}^m(t)} dr \tag{1}$$

where, $\mathbf{B}^m$ is the sum of linear ($\mathbf{B}_L^m$) and nonlinear ($\mathbf{B}_{NL}^m$) strain displacement matrices, $\sigma^m(r,t)$ is the second Piola-Kirchhoff stress, $\mathbf{q}^m(t)$ is the global displacement vector, A^m is the uniform cross section and l^m is the length of element m. Numerical integration is obtained through Gauss-Quadrature method with one Gauss-point. Further, the governing differential equation (gde) for tensegrity is defined by the following,

$$\mathbf{M}\ddot{\mathbf{q}}(t) + \mathbf{C}(t)\dot{\mathbf{q}}(t) + \mathbf{K}(t)\mathbf{q}(t) = \mathbf{f}(t) \tag{2}$$

with $\mathbf{M}$ being the time invariant global mass matrix, $\mathbf{K}(t)$ is the global tangential stiffness, and $\mathbf{C}(t)$ is the Rayleigh damping [4]. External ambient force, $\mathbf{f}(t)$ is modeled as zero mean white Gaussian noise (WGN). $\mathbf{q}(t)$, $\dot{\mathbf{q}}(t)$ and $\ddot{\mathbf{q}}(t)$ are $n \times 1$ order displacement, velocity and acceleration response at the nodes.

3 Substructuring approach

For substructure estimation with Bayesian filters, the sub-domain needs to be decoupled from the rest and be posed as an independent system. *Gde* of the full domain

(Ω), can further be decomposed for N_s independent non-overlapping sub-domain $\{\Omega^s\}$, $s = 1, 2. \cdots, N_s$, denoted as substructures. Each substructure Ω^s can further be defined with two domains: internal Ω^{s_i} and interface boundary Ω^{s_b} involving n_i and n_b internal and boundary *degrees of freedom* (*dof*s) respectively. Except for the nodes lying on Ω^{s_b}, all the nodes of the component substructures belong exactly to one substructure. Accordingly, the *gde* for s^{th} substructure can be isolated as:

$$\begin{bmatrix} \mathbf{M}^s_{ii} & \mathbf{M}^s_{ib} \\ \mathbf{M}^s_{bi} & \mathbf{M}^s_{bb} \end{bmatrix} \begin{Bmatrix} \ddot{\mathbf{q}}^s_i \\ \ddot{\mathbf{q}}^s_b \end{Bmatrix} + \begin{bmatrix} \mathbf{C}_{ii} & \mathbf{C}_{ib} \\ \mathbf{C}_{bi} & \mathbf{C}_{bb} \end{bmatrix} \begin{Bmatrix} \dot{\mathbf{q}}^s_i \\ \dot{\mathbf{q}}^s_b \end{Bmatrix} + \begin{bmatrix} \mathbf{K}_{ii} & \mathbf{K}_{ib} \\ \mathbf{K}_{bi} & \mathbf{K}_{bb} \end{bmatrix} \begin{Bmatrix} \mathbf{q}^s_i \\ \mathbf{q}^s_b \end{Bmatrix} = \begin{Bmatrix} \mathbf{f}^s_i \\ \mathbf{f}^s_b \end{Bmatrix} + \begin{Bmatrix} \mathbf{0} \\ \mathbf{g}^s_b \end{Bmatrix} \quad (3)$$

where subscript i and b signifies internal and boundary *dof*s of order n_i and n_b respectively and superscript s denotes the pertinent substructure. The notation to denote time dependence (i.e., (t)) of the variables are dropped for the sake of readability. Decoupling the dynamics of the substructure s is achieved by compensating with the interface forces $\mathbf{g}^s_b(t)$. The equivalence between global model and the component substructures is ensured through compatibility and equilibrium conditions. While compatibility ensures that the substructures have identical displacements in the connected *dof*s, the force equilibrium condition enforces that forces at the boundary *dof*s of neighbouring substructures cancel each other (c.f. [10] for the details).

From Equation 3, the dynamics of the internal *dof*s can further be decoupled as:

$$\mathbf{M}^s_{ii}\ddot{\mathbf{q}}^s_i + \mathbf{C}^s_{ii}\dot{\mathbf{q}}^s_i + \mathbf{K}^s_{ii}\mathbf{q}^s_i = \mathbf{f}^s_i - \mathbf{M}^s_{ib}\ddot{\mathbf{q}}^s_b + \mathbf{C}^s_{ib}\dot{\mathbf{q}}^s_b + \mathbf{K}^s_{ib}\mathbf{q}^s_b \quad (4)$$

with the right side of Equation 4 collectively considered as external force acting on the substructure, s. [7] further represented the responses at internal *dof*s, i.e., $\mathbf{q}^s_i(t)$, as a summation of a "quasi-static" ($\mathbf{q}^{s,d}_i$) and a "relative" ($\mathbf{q}^{s,r}_i$) components. $\mathbf{q}^{s,d}_i$ can further be obtained by forcing all the force components and time-derivative terms in Equation 3 to zero while assuming the boundary to be free [7],

$$\mathbf{q}^{s,d}_i = -\mathbf{K}^{s\,-1}_{ii}\mathbf{K}^s_{ib}\mathbf{q}^s_b = \eta^s\mathbf{q}^s_b \quad (5)$$

Here η^s can be considered as a transmissibility matrix correlating boundary to internal responses. Next, substituting $\mathbf{q}^s_i(t)$ in Equation 4 with $\mathbf{q}^{s,d}_i$ and $\mathbf{q}^{s,r}_i$, and ignoring the negligible damping forces, the following can be obtained,

$$\mathbf{M}^s_{ii}\ddot{\mathbf{q}}^{s,r}_i + \mathbf{C}^s_{ii}\dot{\mathbf{q}}^{s,r}_i + \mathbf{K}^s_{ii}\mathbf{q}^{s,r}_i = \mathbf{f}^s_i - (\mathbf{M}^s_{ib} + \mathbf{M}^s_{ii}\eta^s)\ddot{\mathbf{q}}^s_b \quad (6)$$

and in state space form with $\mathbf{F}^s(t)_{2n_i\times 2n_i} = \begin{bmatrix} \mathbf{0}_{n_i} & \mathbf{I}_{n_i} \\ -\mathbf{M}^{s\,-1}_{ii}\mathbf{K}^s_{ii} & -\mathbf{M}^{s\,-1}_{ii}\mathbf{C}^s_{ii} \end{bmatrix}$, $\mathbf{B}^s(t)_{2n_i\times n_i} = \begin{bmatrix} \mathbf{0}_{n_i} \\ \mathbf{M}^{s\,-1}_{ii} \end{bmatrix}$, $\mathbf{E}^s(t)_{2n_i\times n_b} = \begin{bmatrix} \mathbf{0}_{n_i} \\ -(\mathbf{M}^{s\,-1}_{ii}\mathbf{M}^s_{ib} + \eta^s) \end{bmatrix}$, $\mathbf{u}(t) = \mathbf{f}^s_{i\ n_i\times 1}$ and $\mathbf{x}^s(t)_{2n_i\times 1} = \begin{Bmatrix} \mathbf{q}^{s,r}_i \\ \dot{\mathbf{q}}^{s,r}_i \end{Bmatrix}$ as,

$$\dot{\mathbf{x}}^s(t) = \mathbf{F}^s(t)\mathbf{x}^s(t) + \mathbf{B}^s(t)\mathbf{u}^s(t) + \mathbf{E}^s(t)\ddot{\mathbf{q}}_b^s(t) + \mathbf{v}^s(t) \tag{7}$$

The additional term $\mathbf{v}^s(t)_{2n_i \times 1}$ represents process uncertainty originating from model inaccuracies and unmodelled inputs. The measurable acceleration responses $\ddot{\mathbf{q}}_i^s$ correspond to total acceleration due to pseudo-static ($\ddot{\mathbf{q}}_i^{s,d}$) and relative ($\ddot{\mathbf{q}}_i^{s,r}$) response components combined as $\mathbf{y}^s(t)_{m\times 1}$,

$$\begin{aligned} \mathbf{y}^s(t) &= \ddot{\mathbf{q}}_i^{s,r} + \ddot{\mathbf{q}}_i^{s,d} = \dot{\mathbf{q}}_i^{s,r} + \eta^s \ddot{\mathbf{q}}_b^s(t) \\ &= \mathbf{S}\{\mathbf{H}^s\mathbf{x}^s(t) + \mathbf{D}^s\mathbf{u}^s(t) + \mathbf{L}^s\ddot{\mathbf{q}}_b^s(t) + \mathbf{w}^s(t)\} \end{aligned} \tag{8}$$

Here, $\mathbf{H}^s_{n_i \times 2n_i} = \begin{bmatrix} -\mathbf{M}_{ii}^{s\,-1}\mathbf{K}^s{}_{ii} & -\mathbf{M}_{ii}^{s\,-1}\mathbf{C}^s_{ii} \end{bmatrix}$, $\mathbf{D}^s = \mathbf{M}_{ii}^{-1}$, $\mathbf{L}^s = -\mathbf{M}_{ii}^{-1}\mathbf{M}_{ib}$ and $\mathbf{w}^s(t)$ denoting measurement noise. $\mathbf{S}_{m\times n_i}$ represents the Boolean selection matrix defining the measured *dof*s. Since in reality, responses are discretely sampled, Equation 7 and 8 can also be presented in discrete time with continuous variables reproduced with their corresponding discrete time entities.

$$\begin{aligned} \mathbf{x}_k^s &= \mathbf{F}_k^s\mathbf{x}_{k-1}^s + \mathbf{B}_k^s\mathbf{u}_k^s + \mathbf{E}_k^s\ddot{\mathbf{q}}_{b,k}^s + \mathbf{v}_k^s \\ \mathbf{y}_k^s &= \mathbf{H}_k^s\mathbf{x}_k^s + \mathbf{D}_k^s\mathbf{u}_k^s + \mathbf{L}_k^s\ddot{\mathbf{q}}_{b,k}^s + \mathbf{w}_k^s \end{aligned} \tag{9}$$

Evidently, the s^{th} substructure can be isolated from the full system domain and estimated independently using measurements recorded from the substructure domain only.

4 Output injection approach

To eliminate the requirement of the interface measurement, $\ddot{\mathbf{q}}_{b,k}^s$, [11]'s output injection technique can be exploited. By suitably injecting a part of the measured output in the state transition model, the state transition can be made independent of $\ddot{\mathbf{q}}_{b,k}^s$. Owing to the measurement equation (cf. Equation (9)), the following holds true for an arbitrary bounded matrix $\mathbf{G}_k^s \in \mathbb{R}^{2n_i \times m}$,

$$0 = \mathbf{G}_k^s\left(\mathbf{y}_k^s - \mathbf{H}_k^s\mathbf{x}_k^s - \mathbf{D}_k^s\mathbf{u}_k^s - \mathbf{L}_k^s\ddot{\mathbf{q}}_{b,k}^s - \mathbf{w}_k^s\right) \tag{10}$$

Adding Equation (9) with Equation (10) and further setting $\mathcal{L}_k^s = \mathbf{I}_{2n_i} - \mathbf{G}_k^s\mathbf{H}_k^s$, Equation (9) can be modified as,

$$\begin{aligned} \mathbf{x}_k^s &= \mathbf{F}_k^s\mathbf{x}_{k-1}^s + \mathbf{B}_k^s\mathbf{u}_k^s + \mathbf{E}_k^s\ddot{\mathbf{q}}_{b,k}^s + \mathbf{v}_k^s + \mathbf{G}_k^s\left(\mathbf{y}_k^s - \mathbf{H}_k^s\mathbf{x}_k^s - \mathbf{D}_k^s\mathbf{u}_k^s - \mathbf{L}_k^s\ddot{\mathbf{q}}_{b,k}^s - \mathbf{w}_k^s\right) \\ &= \tilde{F}_k^s\mathbf{x}_{k-1}^s + \tilde{B}_k^s\mathbf{u}_k^s + \tilde{E}_k^s\ddot{\mathbf{q}}_{b,k}^s + \mathbf{G}_k^s\mathbf{y}_k^s + \tilde{\mathbf{v}}_k^s \end{aligned} \tag{11}$$

with $\tilde{F}_k^s = \mathcal{L}_k^s\mathbf{F}_k^s$, $\tilde{B}_k^s = \mathcal{L}_k\mathbf{B}_k^s - \mathbf{G}_k^s\mathbf{D}_k^s$, $\tilde{E}_k^s = \mathcal{L}_k^s\mathbf{E}_k^s - \mathbf{G}_k^s\mathbf{L}_k^s$ and $\tilde{\mathbf{v}}_k = \mathbf{v}_k^s - \mathbf{G}_k^s\mathbf{w}_k^s$. If $\mathbf{G}_k^s$ is chosen such that $\mathbf{G}_k^s = \mathbf{E}_k^s(\mathbf{H}_k^s\mathbf{E}_k^s + \mathbf{L}_k^s)^\dagger$, with $\dagger$ denoting Moore-Penrose

Pseudo-inverse operation, $\tilde{E}_k^s$ renders to a null matrix and Equation (11) will be robust to $\ddot{\mathbf{q}}_{b,k}^s$. Thus, substructure s can be estimated without measuring the interface response.

STATE AND PARAMETER ESTIMATION - IPENKF

With the substructured system definition, interacting filtering is employed for simultaneous estimation of system parameters, θ and response states $\mathbf{x}_k^s$. Relative efficiency of the conditional estimation through interacting filtering approaches has already been established [2]. Following the interacting filtering technique for tenseg-rity [4], state and parameters are estimated for s^{th} substructure (notation dropped for readability). The PF estimates the parameters while the EnKF nested inside the PF, estimates the state variables. Initially, particle evolution in time is considered as a Gaussian perturbation around the current estimate of the particle $\boldsymbol{\theta}_{k-1}^h$,

$$\boldsymbol{\theta}_k^h = \alpha \boldsymbol{\theta}_{k-1}^h + \mathcal{N}(\delta\boldsymbol{\theta}_k; \boldsymbol{\sigma}_k^{\boldsymbol{\theta}}) \tag{12}$$

where, α is a hyper-parameter that controls the turbulence in the estimation. The particles, are then put through the nested EnKF for state estimation. Within EnKF, N_e state ensembles are propagated through the system (cf. Equation (9)). For this, current estimate for the stiffness matrix $\mathbf{K}_k$ is obtained, (cf. Equation (1)), and prior state ensembles are propagated to the next time step, $\mathbf{x}_{k|k-1}^{g,h}$. Subsequently, the propagated ensembles are observed through measurement predictions, $\mathbf{y}_{k|k-1}^{g,h}$, (cf. Equation (9)).

Next, the predicted measurement, $\mathbf{y}_{k|k-1}^{g,h}$, is compared with the actual measure-ment and innovation $\epsilon_k^{g,h}$ is obtained. Further, ensemble mean of innovation, ϵ_k^h, prop-agated state estimates, $\mathbf{x}_{k|k-1}^h$, and predicted measurements, $\mathbf{y}_{k|k-1}^h$, are obtained with the measurement prediction covariance, $C_k^{h,yy}$ and cross-covariance, $C_k^{h,xy}$ [4].

The innovation error covariance, $\mathbf{S}_k^h$, and EnKF gain, $\mathbf{G}_k^h$, are then obtained as $\mathbf{S}_k^h = C_k^{h,\mathbf{yy}} + \mathbf{R}$ and $\mathbf{G}_k^h = C_k^{h,\mathbf{xy}}(\mathbf{S}_k^h)^{-1}$. With this gain, the state ensembles are updated as,

$$\mathbf{x}_{k|k}^{g,h} = \mathbf{x}_{k|k-1}^{g,h} + \mathbf{G}_k^h \epsilon_k^{g,h} \tag{13}$$

Finally, likelihood of each particle, i.e. $\mathcal{L}(\boldsymbol{\theta}_k^h)$, is calculated based on the innovation mean, ϵ_k^h, and co-variance, $\mathbf{S}_k^h$ following,

$$\mathcal{L}(\boldsymbol{\theta}_k^h) = \frac{1}{(2\pi)^n \sqrt{|\mathbf{S}_k^j|}} e^{-0.5 {\epsilon_k^j}^T {\mathbf{S}_k^j}^{-1} \epsilon_k^j} \tag{14}$$

The normalized weight for each h^{th} particle is further obtained using corresponding likelihood,

$$w(\boldsymbol{\theta}_k^h) = \frac{w(\boldsymbol{\theta}_{k-1}^h)\mathcal{L}(\boldsymbol{\theta}_k^h)}{\sum_{j=1}^{N} w(\boldsymbol{\theta}_{k-1}^h)\mathcal{L}(\boldsymbol{\theta}_k^h)} \tag{15}$$

The particle approximations for the states and parameters are then estimated as their weighted mean.

5 Numerical Experiment

In the following, the proposed algorithm is tested on a 6-stage tensegrity tower, which is composed of 18 bars and 81 cables (cf. Figure 1). The coordinates, and connectivity and element type details are given in Table 1 and Table 2, respectively.

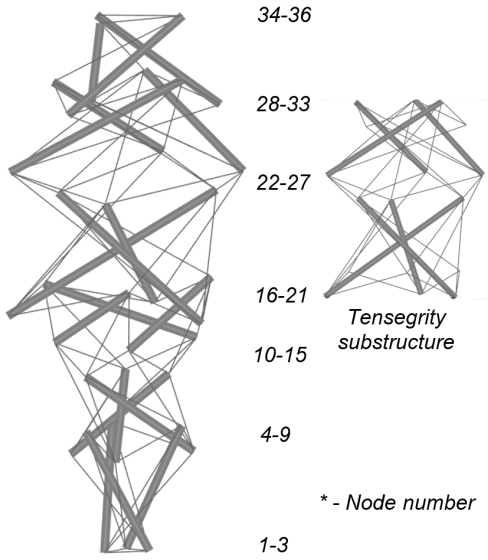

Fig. 1: 6-stage tensegrity tower and tensegrity substructure.

Initial distribution type for **HI**s is set as Gaussian, with a mean of 1 (undamaged) and a standard deviation of 0.02, with α chosen as 0.90 (cf. Equation (12)). For clarity, the **HI** of the damaged member is compared to the **HI** (= 1) of undamaged member 57. 1500 filter particles are selected for PF while 50 ensembles are chosen for EnKF.

Table 1: Nodal coordinates of 6-stage tensegrity tower.

Node	1	2	3	4	5	6	7	8	9	10	11	12
X	0.031	0.029	-0.06	-0.11	-0.054	0.164	0.09	-0.13	0.04	0.19	-0.098	-0.093
Y	0.052	-0.053	0.001	-0.126	0.158	-0.033	-0.098	-0.028	0.127	-0.003	-0.164	0.166
Z	-0.03	-0.03	-0.03	0.002	0.002	0.002	0.012	0.012	0.012	0.04	0.04	0.04
Node	13	14	15	16	17	18	19	20	21	22	23	24
X	0.057	0.054	-0.112	0.204	-0.034	-0.199	-0.112	0.23	-0.118	-0.258	0.265	0.094
Y	0.096	-0.097	0.002	0.201	-0.381	0.2	0.181	-0.003	-0.198	0.099	0.261	-0.359
Z	0.03	0.03	0.03	0.05	0.05	0.05	0.06	0.06	0.06	0.1	0.1	0.1
Node	25	26	27	28	29	30	31	32	33	34	35	36
X	-0.155	-0.055	0.21	-0.207	0.04	0.167	0.045	-0.172	0.127	0.113	-0.113	0
Y	-0.153	0.211	-0.058	-0.073	0.216	-0.142	-0.173	0.047	0.125	-0.065	-0.065	0.13
Z	0.09	0.09	0.09	0.12	0.12	0.12	0.13	0.13	0.13	0.15	0.15	0.15

Table 2: Elemental connectivity and type - 6-stage tensegrity tower.

Element	1	2	3	4	5	6	7	8	9	10	11	12	13	14	15	16	17	18	19	20	21	22	23	24	25
Node 1	1	2	1	1	1	2	2	3	3	4	6	4	5	5	6	5	6	4	6	4	5	10	12	10	11
Node 2	2	3	3	4	8	5	9	6	7	7	7	8	8	9	9	13	11	12	14	15	10	13	13	14	14
Type	c																								
Element	26	27	28	29	30	31	32	33	34	35	36	37	38	39	40	41	42	43	44	45	46	47	48	49	50
1st Node	12	11	10	11	12	13	14	15	16	18	16	17	17	18	16	17	18	19	20	21	22	24	22	23	23
2nd Node	15	15	20	21	19	19	20	21	19	19	20	20	21	21	26	27	25	25	26	27	25	25	26	26	27
Type	c																								
Element	51	52	53	54	55	56	57	58	59	60	61	62	63	64	65	66	67	68	69	70	71	72	73	74	75
1st Node	24	23	24	22	24	22	23	28	30	28	29	29	30	28	32	29	33	30	31	34	35	34	7	8	9
2nd Node	27	31	29	30	32	33	28	31	31	32	32	33	33	34	34	35	35	36	36	35	36	36	15	13	14
Type	c																								
Element	76	77	78	79	80	81	82	83	84	85	86	87	88	89	90	91	92	93	94	95	96	97	98	99	
1st Node	25	26	27	16	17	18	1	2	3	4	5	6	10	11	12	16	17	18	22	23	24	28	29	30	
2nd Node	33	31	32	24	22	23	7	8	9	13	14	15	19	20	21	25	26	27	31	32	33	34	35	36	
Type	c							b																	

A 70% damage is induced in the 51^{st} member, $0.1s$ after the simulation starts. A substructure including nodes 16-33 is selected, which houses the damage member (elem 51). Acceleration data is obtained from internal *dof*s only (corresponding to nodes 22-27 in x- , y-, z- directions), and sampled at 100 Hz for 10.24 seconds. The tensegrity tower is fixed at its bottom nodes (1-3) with ambient Gaussian force applied on all free *dof*s.

Figure 2 shows the proposed algorithm's capability of detecting and quantifying damage in the structure while using substructural information only. An **HI** of about 0.3 is estimated for the 51^{st} element that corresponds to the induced 70% damage. The proposed algorithm is found to be precise and accurate in detecting damage in the substructure, with a single false positive alarm in elem 76 which is in close vicinity of the damaged member. Further, the promptness of the algorithm can be improved by increasing the number of particles and ensembles [4].

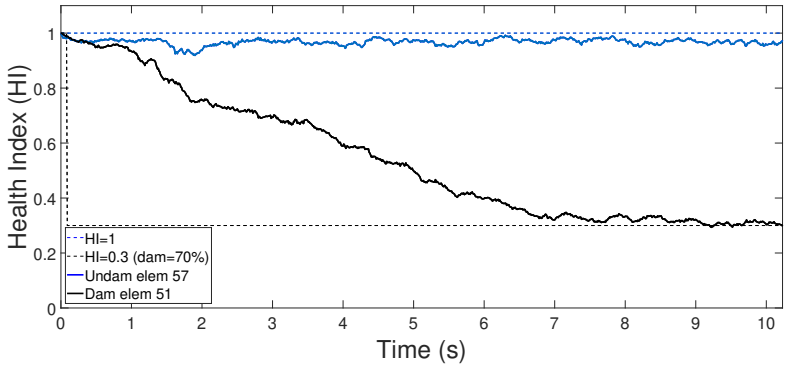

Fig. 2: Damage detection by the proposed approach - Tensegrity substructure.

6 Conclusion

SHM of large complex structures requires substantial amount of computational resources and dense (and therefore costly) instrumentation. Instead, analysing only the critical part of the structure, to monitor its health, can be an efficient option. However since classical substructuring requires the interface (such as boundary force/displacements) to be measured, its integration within traditional SHM approaches are complicated. Hence a novel approach is proposed in the context of tensegrity SHM in which substructure interface measurement has been circumvented with an output injection approach following [11]. While with substructure, the imperative need of monitoring complete structural domain has been avoided, the employment of output injection approach is also benefited with reduction in the required sensor densities. Overall, the proposed method is found to be accurate, precise and prompt based on its performance on a numerical 6-stage tensegrity tower.

Funding: This study was funded by Science & Engineering Research Board (SERB), New Delhi, India, through grant file no. ECR/2018/001464.

References

1. N. Aswal and S. Sen, "Design and health monitoring of tensegrity structures: An overview," in *Reliability, Safety and Hazard Assessment for Risk-Based Technologies*, pp. 523–533, Springer, 2020.
2. R. Karlsson, T. Schon, and F. Gustafsson, "Complexity analysis of the marginalized particle filter," *IEEE Transactions on Signal Processing*, vol. 53, no. 11, pp. 4408–4411, 2005.
3. M. Zghal, L. Mevel, and P. Del Moral, "Modal parameter estimation using interacting kalman filter," *Mechanical Systems and Signal Processing*, vol. 47, no. 1-2, pp. 139–150, 2014.
4. N. Aswal, S. Sen, and L. Mevel, "Estimation of local failure in tensegrity using interacting particle-ensemble kalman filter," *Mechanical Systems and Signal Processing*, vol. 160, p. 107824, 2021.
5. D. de Klerk, D. J. Rixen, and S. Voormeeren, "General framework for dynamic substructuring: history, review and classification of techniques," *AIAA journal*, vol. 46, no. 5, pp. 1169–1181, 2008.
6. J. Hou, Ł. Jankowski, and J. Ou, "An online substructure identification method for local structural health monitoring," *Smart materials and structures*, vol. 22, no. 9, p. 095017, 2013.
7. C. Koh, B. Hong, and C. Liaw, "Substructural and progressive structural identification methods," *Engineering structures*, vol. 25, no. 12, pp. 1551–1563, 2003.
8. J. Hou, Ł. Jankowski, and J. Ou, "A substructure isolation method for local structural health monitoring," *Structural Control and Health Monitoring*, vol. 18, no. 6, pp. 601–618, 2011.
9. A. Souid, A. Delaplace, F. Ragueneau, and R. Desmorat, "Pseudodynamic testing and nonlinear substructuring of damaging structures under earthquake loading," *Engineering structures*, vol. 31, no. 5, pp. 1102–1110, 2009.
10. K. E. Tatsis, V. K. Dertimanis, C. Papadimitriou, E. Lourens, and E. N. Chatzi, "A general substructure-based framework for input-state estimation using limited output measurements," *Mechanical Systems and Signal Processing*, vol. 150, p. 107223, 2021.
11. Q. Zhang and L. Zhang, "State estimation for stochastic time varying systems with disturbance rejection," *IFAC-PapersOnLine*, vol. 51, no. 15, pp. 55–59, 2018.